Chemical Engineering Science, Vol. 46, No. 12, pp. 3067–3080, 1991.
Printed in Great Britain.

0009–2509/91 $3.00 + 0.00
© 1991 Pergamon Press plc

MODELLING AND ANALYSIS OF CVD PROCESSES IN POROUS MEDIA FOR CERAMIC COMPOSITE PREPARATION

Y. S. LIN† and A. J. BURGGRAAF‡
Laboratory of Inorganic Chemistry, Materials Science and Catalysis, Department of Chemical Technology, University of Twente, P.O. Box 217, 7500 AE Enschede, The Netherlands

(*First received* 10 *September* 1990; *accepted in revised form* 28 *February* 1991)

Abstract—A continuum phenomenological model is presented to describe chemical vapour deposition (CVD) of solid product inside porous substrate media for the preparation of reinforced ceramic-matrix composites [by the chemical vapour infiltration (CVI) process] and ceramic membrane composites (by a modified CVD process). The chemical reaction, intrapore diffusion, non-isobaric viscous flow and variation of substrate pore geometry during deposition are considered in the model which is readily solved by the orthogonal collocation numerical technique. Simulated deposition profiles across substrate are given to examine the effects of the reaction mechanism, reaction and diffusion rate, substrate pore dimension, deposition temperature, bulk phase reactant concentration, intrapore diffusivity of reactants and pressure drop on the deposition results of a one-dimensional isothermal forced-flow CVI process and a modified non-isobaric CVD process for ceramic composite preparation. The theoretical analysis provides a better insight of the CVD processes in porous media and is useful in explaining experimental findings and guiding the selection of optimum process conditions for the CVD preparation of ceramic composites.

INTRODUCTION

Ceramic composite materials represent one of the most important developments in materials science and technology. Among these materials the reinforced ceramic-matrix composites are gaining technical importance in aerospace, automobile and manufacturing industries because of their unique characteristics in oxidation resistance, low density and refractory properties (Naslain *et al.*, 1989; Chiang *et al.*, 1989). On the other hand, the potential of ceramic membrane composites in gas separation, purification and catalytic reaction processes due to their high structural and thermal stability, long life in application and capability of having catalytic properties have recently stimulated increasing research in the synthesis and property improvement of these inorganic membranes (cf. Keizer *et al.*, 1988; Hsieh, 1988; Burggraaf *et al.*, 1989; Burggraaf and Keizer, 1990). However, the controlled preparation of the ceramic-matrix composites and membrane composites with a top-layer in sub-nanometer scale pore size presents some of the most difficult processing problems in the ceramic fields. The recent development in extending the chemical vapour deposition (CVD) method into porous ceramic substrates has demonstrated that the CVD approach is one of the most promising reaction-forming processes for making these ceramic composites.

The CVD approach for ceramic-matrix composite preparation has been studied for more than one decade (cf. Christin *et al.*, 1979; Rossignol and Naslain 1980). In comparison, the CVD approach has just been very recently applied to the preparation (Gavalas *et al.*, 1989) and modification (Lin *et al.*, 1989a) of ceramic membrane systems. In principle, the CVD processes for the preparation of the ceramic-matrix composites and ceramic membranes have a number of aspects in common. In these CVD processes selected vapour reactants (or reactant) are introduced into internal substrate pore space by means of diffusion and/or forced viscous flow and a desired solid product is deposited on the internal pore surface of the porous substrate. For ceramic-matrix composites the porous substrates are usually coarse porous ceramic-matrix preforms (e.g. carbon fiber matrix) in which a solid of the same material (e.g. carbon) or different material (e.g. silicon carbide) is deposited for densification. The substrates can be, for membrane preparation, coarse-pore ceramic discs (or tubes) (e.g. α-alumina) in which a thin-layer with membrane property is formed (Gavalas *et al.*, 1989), and for membrane modification, a ceramic membrane composite with a small pore top-layer in which the pores are modified by the CVD to improve the membrane property (Lin *et al.*, 1989a, b).

There are two major differences between the CVD process for the preparation of ceramic-matrix composite and the CVD process for the preparation or modification of ceramic membrane. The first is the introduction of the reactants into the porous substrates. For the preparation of ceramic-matrix composite, the reactants are introduced from the same side of the preform and therefore this CVD process is referred to in literature as the chemical vapor infiltration (CVI). For membrane preparation or modification, two reactants are introduced from opposite sides of substrate and to differentiate from the CVI this

†Present address: Department of Chemical Engineering, University of Cincinnati, Cincinnati, OH 45221, U.S.A.
‡Author to whom correspondence should be addressed.

CVD process is hereby referred to as the modified CVD (MCVD). This can be more easily visualized in Fig. 1. The second difference arises from the requirement of the distribution of deposited solid product across the substrates. In the CVI process a uniform distribution of the solid deposit across the substrate is desired in order to achieve the best mechanical property of the ceramic-matrix composites. In the MCVD process, however, a deposition zone as narrow as possible is preferred in order to reduce the transport resistance while retaining the high selectivity. To increase the deposition rate and/or the uniformity of the solid deposit distribution, a total pressure drop or a temperature gradient is imposed on the preform for making ceramic-matrix composites. This results in the non-isothermal and/or forced-flow CVI (Besmann *et al.*, 1989). It should be mentioned that the MCVD process is also the initial stage of the electrochemical vapour deposition of thin dense solid electrolyte films on porous substrate for the fabrication of solid oxide fuel cells and dense membranes (Isenburg, 1977; Carolan and Michaels, 1990; Lin *et al.*, 1990c).

The CVI process has been more extensively studied by experiments. In comparison, the theoretical studies on the CVI are limited. The earlier attempt on the theoretical analysis of the one-dimensional CVI process can be found in the work of Brekel *et al.* (1981) who presented an approximate solution describing the deposition profiles within cylindrical tubes of small diameter (0.1–1 mm). This theoretical analysis was later extended by Rossignol *et al.* (1984) to estimate the deposition profiles of TiC inside a carbon–carbon composite preform. The analysis was made for isothermal non-forced flow CVI using a mathematical model considering only diffusion and

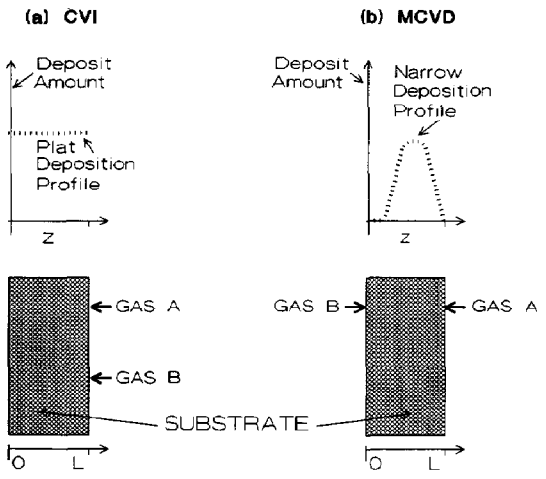

Fig. 1. Schematic illustration of the one-dimensional CVI process for material densification (a) in which a flat deposition profile is desired and the MCVD process for membrane preparation (b) in which a narrow deposition profile is preferred.

decomposition of one reactant in the preform. A more detailed analysis on the isothermal, non-forced flow CVI process for growth of Al_2O_3 in SiC fiber preform was recently reported by Tai and Chou (1988, 1989) based on a model similar to the one of Brekel *et al.* (1981). In this analysis the pore space between SiC fibers was simulated as cylindrical tubes. Axial and radial diffusion of vapour reactants, chemical reaction on the inner surface of the tube and deposition film growth were considered in the model. The above mentioned theoretical work dealt with isothermal non-forced flow CVI process. Gupte and Tsamopoulos (1989) recently published their theoretical analysis on a non-isothermal and isobaric CVI based on a model describing the combined diffusion and reaction of trichloromethylsilane (TMS) and the deposition of silicon carbide in porous preform. The mass transport of TMS in an idealized cylindrical pore and heat conduction in the preform were described by two partial differential equations with a moving boundary condition. This complex model was solved by the finite element numerical method to give the simulated deposition profiles.

In the above mentioned continuum models for the one-dimensional CVI processes (Brekel *et al.*, 1981; Tai and Chou, 1988, 1989; Gupte and Tsamopoulos, 1989), the variation of the pore cross-sectional area, pore size and diffusivity during the CVI process was not taken into account in deriving the transport equation. In reality the CVI is a process with changing substrate geometry and transport properties. In contrast, the diffusion in pore radial direction which can be more reasonably neglected due to larger pore length/size ratio was considered, yielding a much more complex partial differential equation of three variables (pore axial position, pore radius and time). Furthermore no viscous flow was considered in these models and, as a result, these continuum models could not be used to study non-isobaric CVI processes. Following a different approach Starr (1987, 1988) developed a stage model for the prediction of the densification–deposition time relation of a non-isothermal forced-flow CVI. In this model a preform was divided into a finite number of volume elements, in each of which the preform structure, thermal conductivity and other physical parameters were assumed to be constant. Based on this model an iteration algorithm was used to calculate the average density of the preform under the CVI process as a function of deposition time. This model offers a simpler approach for the theoretical analysis, but is less realistic for the continuous CVD process in porous media.

The theoretical analysis of the MCVD process for membrane preparation and modification are even scarce. Carolan and Michaels (1987), in an attempt to understand the penetration depth of a deposit into a porous substrate in the initial stage of the electrochemical vapour deposition of dense electrolyte film, reported a simple continuum model to predict the deposition profile across substrate. Again, variation of the substrate pore geometry during deposition and its

effect on the intrapore diffusivity were not considered in the model. Furthermore this model only analyses isobaric MCVD process. Lin *et al.* (1989b) recently presented some preliminary simulation and experimental results on the deposition of zirconia (as well as yttria) on porous substrate disc for membrane preparation. The simulation was based on an improved continuum model which includes chemical reaction, diffusion and viscous flow in substrate pores. In both the studies of Carolan and Michaels (1987) and Lin *et al.* (1989b), the boundary conditions of zero reactant concentration at the corresponding pore exit were used to simplify computation. The simulation results were consistent with some of the experimentally measured deposition profiles but failed to explain other experimental evidences (Lin *et al.*, 1990a) due to mainly the improper use of the boundary conditions.

In the present paper, a more complete mathematical model and analysis are presented for the one-dimensional CVI and the MCVD processes for the preparation of reinforced ceramic-matrix composite and ceramic membranes. As there has been no effort reported using one model to describe the CVI and MCVD processes which are very different as far as the distribution of deposit is concerned, the main objectives of the present work are to report a comparative analysis of the CVI and MCVD processes by the same model and the parametric study on these two CVD processes using the simulation results.

MATHEMATICAL MODELLING

Model development

A realistic mathematical description of mass transport in the CVI and MCVD processes is complicated by the undefined pore structure of porous ceramic substrates. Thus, to obtain a continuum model the CVD processes in porous media can be phenomenologically described as simultaneous diffusion, convection and reaction/deposition in a simplified structure being a one-dimensional cylindrical pore along reactant penetrating direction. This simplified approach is generally used for the study of mass transport in porous media including the previous theoretical work on the CVI and MCVD processes (Brekel *et al.*, 1981; Carolan and Michaels, 1987; Tai and Chou, 1989; Gupte and Tsamopolos, 1989). With this approach the CVI and MCVD processes are considered as deposition of solid in the cylindrical pore with a initial pore radius of R^0 at any axial position Z, as shown in Fig. 2. As the solid product deposits on the wall of the pore, the pore radius changes. The aim of the mathematical modelling then becomes to find the solution of the pore radius as a function of pore axial position and time. In this work, only one-dimensional isothermal forced-flow CVI and non-isobaric MCVD processes with two vapour reactants are considered (see Fig. 2 for the reaction). The following additional assumptions are also made in the modelling: (1) a quasi-steady state for the CVD processes due to the fact that the gas diffusion rate is much faster than the pore narrowing rate; (2) negligible concentration change of the vapour reactants in the pore radial direction due to large ratio of substrate thickness to average substrate pore radius (L/R^0) in most studied ceramic substrate pores; (3) dilute reactant concentration so that the simplified dusty-gas model can be applied with a negligible effect of gaseous reaction products on the pressure gradient.

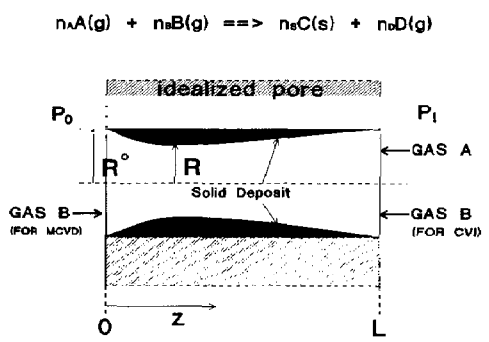

Fig. 2. Cylindrical pore model for modelling CVD processes in porous media.

Mass balance on reactant i over the differential volume of $(\pi R^2)(dZ)$ in the cylindrical pore gives (Bird *et al.*, 1960):

$$-\frac{1}{R^2}\frac{d(J_i R^2)}{dZ} - (-\mathbf{R}_i) = 0 \tag{1}$$

where $(-\mathbf{R}_i)$ is the consumption rate of reactant i based on the unit pore volume; J_i is the mass flux of reactant i at position Z in the substrate pore. If there exists a total pressure gradient over the substrate, this flux, according to the dusty-gas model, consists of a diffusive flux, $J_{i(d)}$, and a viscous flux, $J_{(v)}$ (Mason *et al.*, 1966; Mason and Malinauskas, 1983) as:

$$J_i = J_{i(d)} + x_i J_{(v)} \tag{2}$$

where x_i is the molar fraction of reactant i. Although the complete description of the diffusive flux in porous medium for component i in a multi-component gas system is very complex, for a dilute reactant gas the following relation can be approximately used for $J_{i(d)}$ to simplify the problem (Smith, 1981; Ruthven, 1984):

$$J_{i(d)} = -D_i \frac{dC_i}{dZ} \tag{3}$$

with

$$\frac{1}{D_i} = \frac{\tau}{\varepsilon}\left[\frac{1}{D_{i(m)}} + \frac{1}{D_{i(k)}}\right] \tag{4a}$$

where $D_{i(m)}$ is molecular diffusivity for component i in the carrier gas; $D_{i(k)}$ is the Knudsen diffusivity for species i. Other symbols are identified in the "Notation". The Knudsen diffusivity is related to the average pore radius by (Butt, 1980; Smith, 1981):

$$D_{i(k)} = a_k R \tag{4b}$$

and the molecular diffusivity is correlated to the total pressure by the Champman and Enskog equation (Reid *et al.*, 1975) as:

$$D_{i(m)} = a_m/P \tag{4c}$$

where the coefficients a_k and a_m are functions of temperature and molecular weights of diffusing gas and carrier gas, and can be found in the indicated references.

The viscous flow $J_{(v)}$ can be related to the total pressure gradient as (Bird *et al.*, 1960; Mason *et al.*, 1966):

$$J_{(v)} = -\frac{\varepsilon P B_0}{\tau R_g T \mu}\frac{dP}{dZ} \tag{5}$$

where B_0 is a characteristic constant of the substrate medium (Mason *et al.*, 1966). For a straight cylindrical pore, $B_0 = R^2/8$ (Mason *et al.*, 1966; Mason and Malinauskas, 1983).

Combining eqs (3) and (5) into eq. (2) gives:

$$J_i = -D_i\frac{dC_i}{dZ} + UC_i \tag{6}$$

with

$$U = -\frac{\varepsilon B_0}{\tau\mu}\frac{dP}{dZ} \tag{7}$$

or for the cylindrical pore:

$$U = -\frac{\varepsilon R^2}{8\mu\tau}\frac{dP}{dZ}. \tag{8}$$

As indicated by eqs (4) and (8), both D_i and U are dependent on the pore radius R and total pressure P. Since R and P vary with Z and t during deposition, both D_i and U are also functions of Z and t. Therefore, substituting eq. (6) into eq. (1) results in:

$$D_i\frac{d^2C_i}{dZ^2} + \left[\frac{d(D_iR^2)}{R^2\,dZ} - U\right]\frac{dC_i}{dZ} - \frac{d(UR^2)}{R^2\,dZ}C_i - (-\mathbf{R}_i) = 0. \tag{9}$$

The above mass conservation equation is very different from the previously reported models for the one-dimensional CVI and the MCVD (Brekel *et al.*, 1981; Carolan and Michaels, 1987; Tai and Chou, 1988, 1989; Gupte and Tsamopoulos, 1989). In addition to the inclusion of the viscous flow term in eq. (6), the differences arise from the consideration of changing pore cross-sectional area and the position dependent effective diffusivity in this work, which are more realistic to the described CVD processes. The neglect of changing pore geometry and position dependency of intrapore diffusivity can substantially affect the simulation results for the cases in which the solid is not uniformly deposited across a substrate.

The resulting mass balance eq. (9) applies for the both CVI and MCVD. As described in the Introduction, the phenomenological difference between the CVI and the MCVD is that for the CVI the reactants A and B are introduced from the same side of the substrate while for the MCVD the two reactants are, respectively, introduced from the opposite sides of the substrate. It is more straightforward to show the difference in the boundary conditions (BC) as:

for the CVI process:

$$C_A = C_A^0; \quad C_B = C_B^0 \quad \text{at } Z = L \tag{10}$$

$$\frac{dC_A}{dZ} = 0; \quad \frac{dC_B}{dZ} = 0 \quad \text{at } Z = 0 \tag{11}$$

for the MCVD process:

$$C_A = C_A^0; \quad \frac{dC_B}{dZ} = 0 \quad \text{at } Z = L \tag{12}$$

$$C_B - C_B^0; \quad \frac{dC_A}{dZ} - 0 \quad \text{at } Z - 0. \tag{13}$$

The diffusion directions of reactant A and B in the CVI and MCVD are shown in Fig. 2. Carolan and Michaels (1987) and Lin *et al.* (1989b) imposed a zero concentration for reactant i at the corresponding pore exit for the MCVD process (i.e. $C_A = 0$ at $Z = 0$ and $C_B = 0$ at $Z = L$), while Brekel *et al.* (1981) and many other investigators (e.g. Tai and Chou, 1988, 1989; Gupte and Tsamopoulos, 1989) employed a zero derivative of the reactant i concentration for the BC at the corresponding pore exit. In fact, these two types of BC are the two special cases of a more realistic BC [$dC_i/d\xi = N_{Bi}C_i$, where $\xi = Z/L$ and N_{Bi} is the Biot number (Butt, 1980)] with $N_{Bi} = \infty$ and $N_{Bi} = 0$, respectively. However, the use of the more realistic BC will introduce more parameters (N_{Bi}) whose values for such CVD processes are still unknown. To avoid this problem, the type of BC of Brekel *et al.* (1981), which has been commonly used in CVI modelling, is also used in the present study.

For deposition of solid product on the internal pore surface the two reactants should be adsorbed and then react on the pore wall. Thus, the formation rate of the solid product should be proportional to the pore surface area and the reactant concentration on the pore surface. Assuming uniform concentration over the pore cross-sectional area and using the modified mass action law (Butt, 1980), the formation rate for the solid product is expressed as:

$$\mathbf{R}_s = KC_A^N C_B^M. \tag{14}$$

Note that R_s is defined on the basis of the unit pore surface area while the consumption rate for reactant i in eq. (1) is based on the unit pore volume. $\mathbf{R}_s$ and $\mathbf{R}_i$ can be correlated by:

$$\mathbf{R}_s = (R/2)(n_s/n_i)(-\mathbf{R}_i). \tag{15}$$

It is straightforward to derive the following mass balance equation for the deposition of the solid product:

$$\frac{dR}{dt} = -\mathbf{R}_s\frac{M_s}{\rho} \tag{16}$$

with the initial condition:

$$R = R^0 \qquad \text{at } t = 0. \tag{17}$$

Mass balance on the total flux described by eq. (5) gives in the following equation for the total pressure across the substrate:

$$\frac{\mathrm{d}}{\mathrm{d}Z}\left[\frac{P\,\mathrm{d}P}{\mathrm{d}Z}R^2\right] = 0 \tag{18}$$

with the boundary conditions:

$$P = P_0 \qquad \text{at } Z = 0 \tag{19}$$

$$P = P_1 \qquad \text{at } Z = L. \tag{20}$$

Thus the viscous flow velocity U is related to Z by eq. (7) in which the total pressure gradient $\mathrm{d}P/\mathrm{d}Z$ can be calculated from the simultaneous solution of eq. (18) and other differential equations as presented above. The mathematical model for the CVD processes is complicated by the fact that the coefficients for the differential equations vary with the time and position. Analytical solutions for such a complicated problem is very difficult. Therefore, this problem has to be numerically solved.

Numerical solutions

The above differential equations and boundary conditions are first non-dimensionalized by introducing the dimensionless variables defined in Table 1.

For diffusion and reaction of reactant A and B in substrate pores this results in:

$$A_i\frac{\mathrm{d}^2X_i}{\mathrm{d}\xi^2} + B_i\frac{\mathrm{d}X_i}{\mathrm{d}\xi} + E_iX_i - f_i(X_\mathrm{A}, X_\mathrm{B}) = 0 \tag{21}$$

(with i = A for reactant A and i = B for reactant B) with the BC for the CVI process:

$$X_\mathrm{A} = 1; \qquad X_\mathrm{B} = 1 \qquad \text{at } \xi = 1 \tag{22}$$

$$\mathrm{d}X_\mathrm{A}/\mathrm{d}\xi = 0; \qquad \mathrm{d}X_\mathrm{B}/\mathrm{d}\xi = 0 \qquad \text{at } \xi = 0 \tag{23}$$

and the BC for the MCVD process:

$$X_\mathrm{A} = 1; \qquad \mathrm{d}X_\mathrm{B}/\mathrm{d}\xi = 0 \qquad \text{at } \xi = 1 \tag{24}$$

$$X_\mathrm{B} = 1; \qquad \mathrm{d}X_\mathrm{A}/\mathrm{d}\xi = 0; \qquad \text{at } \xi = 0 \tag{25}$$

for the total pressure gradient:

$$\frac{\mathrm{d}}{\mathrm{d}\xi}\left[\frac{\mathrm{d}Y}{\mathrm{d}\xi}\phi^2\right] = 0 \tag{26a}$$

or in the following form:

$$A_v\frac{\mathrm{d}^2Y}{\mathrm{d}\xi^2} + B_v\frac{\mathrm{d}Y}{\mathrm{d}\xi} = 0 \tag{26b}$$

with the corresponding BC as:

$$Y = 1 \qquad \text{at } \xi = 1 \tag{27}$$

$$Y = 0 \qquad \text{at } \xi = 0. \tag{28}$$

The pore-size narrowing rate eq. (16) is non-dimensionalized to:

$$\mathrm{d}\phi/\mathrm{d}\theta = -f_s(X_\mathrm{A}, X_\mathrm{B}) \tag{29}$$

with the corresponding initial condition:

$$\phi = 1 \qquad \text{at } \theta = 0. \tag{30}$$

It is important to note that the coefficients A_i, B_i, E_i (i = A and B) in eq. (21) and A_v and B_v in eq. (26) are dependent on the dimensionless time and axial position. These coefficients in the dimensionless form are listed in Table 2. The dimensionless concentration terms in eqs (21) and (29), $f_\mathrm{A}(X_\mathrm{A}, X_\mathrm{B})$, $f_\mathrm{B}(X_\mathrm{A}, X_\mathrm{B})$ and $f_s(X_\mathrm{A}, X_\mathrm{B})$ are also listed in Table 2. The definitions of the dimensionless parameters appearing in Table 2 are given in the lower part of Table 1.

The simulated deposition profiles (the dimensionless pore radius ϕ as a function of dimensionless pore axial position, ξ, and deposition time, θ) can be obtained from the simultaneous solutions of the four differential equations [two equations from eq. (21) for

Table 1. Definition of dimensionless variables and parameters

Dimensionless variables	
Pore axial position	$\xi = Z/L$
Pore radius	$\phi = R/R^0$
Deposition time	$\theta = tD^0_\mathrm{A}/L^2$
Concentration	$X_i = C_i/C^0_i$
Total pressure	$Y = (P^2 - P_0^2)/(P_1^2 - P_0^2)$
Viscous flow velocity	$H = UL/D^0_\mathrm{A}$
Dimensionless parameters	
Reaction order on reactant A	N
Reaction order on reactant B	M
Thiele modulus	$\Phi = KL^2(C^0_\mathrm{A})^{N-1}(C^0_\mathrm{B})^M/D^0_\mathrm{A}R^0$
Diffusivity ratio	$\lambda_\mathrm{B} = D^0_\mathrm{B}/D^0_\mathrm{A}$ ($\lambda_\mathrm{A} = 1$)
Reactant concentration ratio	$\beta = C^0_\mathrm{B}/C^0_\mathrm{A}$
Pressure drop coefficient	$\alpha = (P_1^2 - P_0^2)/P_0^2$
Ratio of viscous flow velocity to diffusivity	$\lambda_v = R^{02}P_0\varepsilon/16\mu\tau D^0_\mathrm{A}$
Ratio of Knudsen diffusivity to molecular diffusivity	
Reactant A	$\omega_\mathrm{A} = D^0_{\mathrm{A}(k)}/D^0_{\mathrm{A}(m)}$
Reactant B	$\omega_\mathrm{B} = D^0_{\mathrm{B}(k)}/D^0_{\mathrm{B}(m)}$
Vapour to solid concentration ratio	$\gamma = C^0_\mathrm{A}M_s/\rho$

reactant A and reactant B, and eqs (26) and (29)]. This boundary and initial value problem was solved by the orthogonal collocation numerical method (Villadsen and Michelsen, 1978). In the numerical computation, the four differential equations were discretized along the pore axial coordinate to form $Nc + 2$ algebraic equations from eq. (21) (for component A or B) and eq. (26), respectively, and $Nc + 2$ ordinary differential equations from eq. (29). Here Nc is the total number of the internal collocation points. This resulted in a set of $4(Nc + 2)$ algebraic and differential equations (ADEs). Details on the collocation equations and computation algorithm for numerical solutions are presented in the Appendix. The IMSL routine NEQNF (IMSL, 1987) was used to solve the nonlinear algebraic collocation equations.

A deposition profile at a certain deposition time Θ (e.g. the moment of pore-closure, i.e. $\phi = 0$ at $\xi = 1$ for the CVI) was computed by integrating the differential equation eq. (29) from $\theta = 0$ to Θ coupled with simultaneous solutions of the nonlinear algebraic collocation equations. It should be pointed out that the simulated deposition profile at $\theta = \Theta$ is the result of evolution of the same deposition profile from $\theta = 0$. The Euler's method (Carnahan *et al.*, 1977) with an adjustable step size during integration (typical over 1000 steps used to integrate from $\phi = 1$ to 0.5) was used to solve the differential equations at the different collocation points. A preliminary calculation showed that a simulated deposition profile with $Nc = 10$ or 12 is essentially the same as the simulated deposition profile with $Nc = 8$ but required much more computation time due to the increase in the total number of ADEs. Therefore eight internal collocation points were used in the simulation computation for the results presented in the next section. The typical CPU time required using the VAX 8650 at the University of Twente computer center was about 5 s to obtain one simulated deposition profile at the deposition time Θ at which $\phi_{(\text{minimum})} = 0$.

Table 2. Coefficients and concentration terms for the dimensionless differential equations

Coefficient	Relation to ϕ and Y	
A_i	$= \lambda_i \phi^2 h_i$	(31)
B_i	$= a_i(\mathrm{d}\phi/\mathrm{d}\xi) + b_i H$	(32)
E_i	$= -2H(\mathrm{d}\phi/\mathrm{d}\xi) - \phi(\mathrm{d}H/\mathrm{d}\xi)$	(33)
A_v	$= \phi$	(34)
B_v	$= 2\mathrm{d}\phi/\mathrm{d}\xi$	(35)
$f_A(X_A, X_B)$	$= 2(n_A/n_s)\Phi X_A^N X_B^M$	(36)
$f_B(X_A, X_B)$	$= 2(n_B/n_s)\Phi\beta^{-1} X_A^N X_B^M$	(37)
$f_s(X_A, X_B)$	$= \gamma\Phi X_A^N X_B^M$	(38)
where a_i, b_i, h_i and H are related to ϕ and Y by:		
a_i	$= \lambda_i h_i \phi[h_i/(\omega_i + 1) + 2]$	(39)
b_i	$= 0.5\phi[\omega_i/(\omega_i + 1)](\lambda_i/\lambda_v)h_i^2 - \phi$	(40)
h_i	$= (\omega_i + 1)/[\omega_i\phi(\alpha Y + 1)^{1/2} + 1]$	(41)
H	$= -[\lambda_v \alpha\phi^2/(\alpha Y + 1)^{1/2}](\mathrm{d}Y/\mathrm{d}\xi)$	(42)

RESULTS AND DISCUSSION

The simulation results presented in this section for the MCVD is based on a CVD process for deposition of zirconia into a porous substrate for membrane preparation and modification (Lin *et al.*, 1989a, b). The substrate is an α-alumina disc of 12 mm in diameter and 2 mm in thickness. $ZrCl_4$ vapour and H_2O vapour are used as two reactants and the following CVD reaction is considered to take place in the substrate pores: $ZrCl_4(g)$ (reactant A) + $2H_2O(g)$ (reactant B) = $ZrO_2(s) + 4HCl(g)$. The typical experimental conditions and the corresponding dimensionless parameters for the CVD process are summarized in Table 3. For the sake of comparison the simulation results for the CVI are also based on the same CVD process for membrane modification, as summarized in Table 3 but with a smaller value of the reaction rate constant (or Φ). Although the actual dimension of preforms and reaction conditions for CVI processes may differ from the one presented herein, the simulation results should provide the general picture of the one-dimensional isothermal forced CVI processes because the analysis is made on the dimensionless basis.

To show the effects of the different parameters on the CVD process for ceramic composite preparation, the simulated deposition profiles at the moment of

Table 3. Values of parameters used for simulation

(A) CVD process parameters and experimental conditions	
$R^0 = 1 \times 10^{-7}$ m	$n_A = 1$
$L = 2 \times 10^{-3}$ m	$n_B = 2$
$\varepsilon^0 = 0.5$	$n_s = 1$
$\tau = 4$	$N = 1$
$C_A^0 = 2.0 \times 10^{-3}$ mol/m^3	$M = 1$
$C_B^0 = 3.5 \times 10^{-3}$ mol/m^3	$K = 3.62 \times 10^{-4}$ m^4/s mol (for MCVD)
$D_A^0 = 2.9 \times 10^{-6}$ m^2/s	$K = 3.62 \times 10^{-6}$ m^4/s mol (for CVI)
$D_B^0 = 1.02 \times 10^{-5}$ m^2/s	$T = 1000$°C
$P_0 = 200$ Pa	$\mu = 6.5 \times 10^{-5}$ kg/s m
$P_1 = 200$ Pa	$\rho/M_s = 4.65 \times 10^4$ mol/m^3
(B) Dimensionless parameters calculated from Part A of this table	
$\Phi = 17.5$ (for MCVD)	$\Phi = 0.175$ (for CVI)
$\lambda_B = 3.5$	$\beta = 1.75$
$\alpha = 0$	$\lambda_v = 8 \times 10^{-5}$
$\gamma = 4.3 \times 10^{-8}$	$\omega_i \approx 10^{-4}$

pore closure (for CVI) or that of half-pore-narrowed (for the MCVD) are presented in Figs 4–11. The values of the studied parameter(s) together with the corresponding simulated pore closure time (for the CVI) or half-pore-narrowed time (for the MCVD) are indicated in each figure. The values for all other parameters are the same as given in Table 3 unless otherwise specified in the figure captions. From the simulated deposition profiles one can study the effects of the different parameters on (1) maximum deposition location (at which R is minimum in the deposition profile), (2) broadness of deposition zone and (3) the pore narrowing rate (inversely proportional to half-pore-narrowed time) for membrane preparation. For material densification the simulated deposit profiles, which can be easily converted to porosity–axial position profiles using the relation of $\varepsilon/\varepsilon^0 = \phi^2$, provide information on the effects of different parameters on the uniformity of densification and the densification rate. The experimental study of the effects of several parameters on the MCVD results for membrane preparation and the explanation using the modelling results will be reported in a separate paper.

Figure 3 shows typical simulated profiles of pore radius, reactant concentrations and the total pressure (all in dimensionless form) across the substrate disc for the CVI and the MCVD. Note that X_i is the relative concentration of reactant i with respect to its concentration in the bulk phase. For both reactant A and reactant B the concentration decreases from the pore entrance and levels off near its pore exit. The depletion of the reactants is due to consumption of the reactants by chemical reaction and deposition. It is interesting to note that for the CVI the reactant concentration drops rapidly in the region near the pore entrance ($Z = L$) [Fig. 3(a)] while for the MCVD the reactant concentrations change more significantly in the region where the two concentration profiles cross. As shown by the deposition profiles of $\phi(Z/L)$, the reactant concentrations vary more significantly in the region where more solid is deposited.

Figure 4 illustrates the effects of the reaction mechanism on the deposition profiles for the CVI and MCVD. For an isothermal CVI the maximum deposition location (at which ϕ is smallest) is always at the entrance port (at $Z = L$), as shown in Figs 3(a) and 4(a). For the MVCD, however, the maximum deposition location vary with the different reaction mechanisms, transport properties and experimental conditions. For the case of a zero reaction order with respect to one reactant, the maximum deposition location for the MCVD is at the entrance port for the reactant with a non-zero reaction order, as shown in Fig. 4(b). For the case of non-zero reaction order with respect to both the reactants, the maximum deposition location varies from $Z = 0$ to $Z = L$ depending on the values of other parameters to be discussed later.

The Thiele modulus Φ, as defined in Table 1, can be considered as the ratio of the reaction rate to the diffusion rate. The effects of Φ on the deposition profiles for CVI and MCVD are shown in Fig. 5. For both the processes, a smaller value of Φ results in a flatter deposition profile with a lower pore narrowing rate (or longer pore-closure time). This is because the reactants can penetrate deeper into the substrate

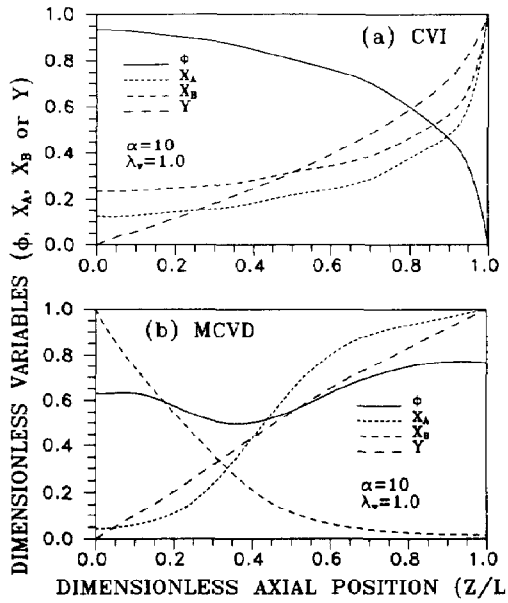

Fig. 3. Simulated profiles of dimensionless pore radius (ϕ), concentrations of two reactants (X_A, X_B) and total pressure (Y) at (a) the moment of pore closure for the CVI and (b) the moment of half pore-narrowed for the MCVD.

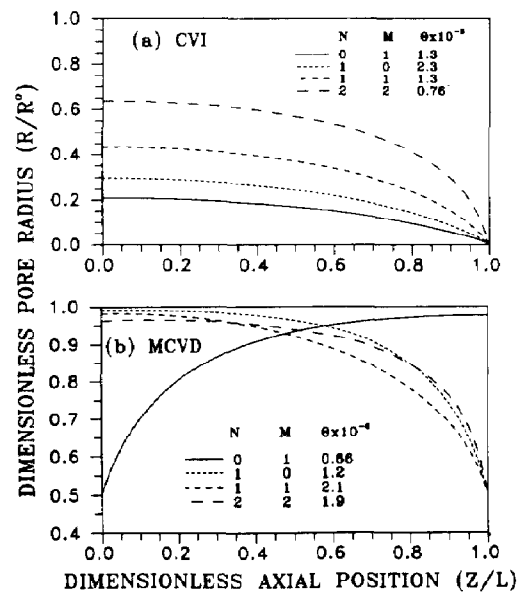

Fig. 4. Effects of the reaction orders of N (with respect to reactant A) and M (to reactant B) on the deposition profiles for (a) the CVI and (b) the MCVD (with all the dimensionless parameter values given in Table 3 part B).

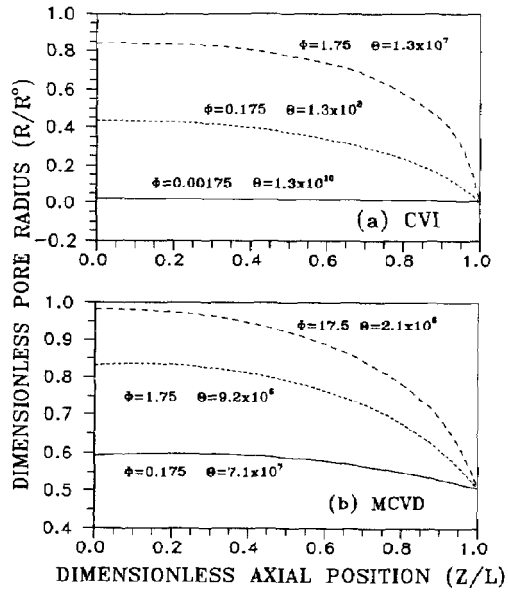

Fig. 5. Effects of Thiele modulus (temperature, pressure, substrate pore dimension, reactant concentration) on the deposition profiles for (a) the CVI and (b) the MCVD (with $N = 1$, $M = 1$ and all other dimensionless parameter values given in Table 3 part B).

pores with a higher diffusion rate and/or lower reaction rate. In general, decreasing the ratio of reaction rate/diffusion rate improves the uniformity of the deposition rate across the substrate but reduces the average pore-narrowing rate. For the CVI it is obvious that the pore-closure time is inversely proportional to Φ, as given in Fig. 5(a). However, the half-pore-narrowed time for the MCVD decreases with increasing Φ but is not inversely proportional to Φ except the case of zero reaction order with respect to one of the reactants.

The Thiele modulus, according to the definition, represents the four important experimental parameters or conditions: deposition temperature, substrate pore dimension, reactant concentrations and total pressure. As the reaction rate constant K in this model lumps together all the rate and equilibrium constants for several steps involved in a CVD reaction/deposition process such as adsorption and surface reaction, the temperature dependence of K varies with different reaction/deposition mechanism. For the Langmuir–Hinshelwood-type reaction mechanism (Butt, 1980) with large heats of adsorption on the substrate internal surface, K and hence the Thiele modulus decrease with temperature. When the surface reaction with a relatively large activation energy E_a is the rate-limiting step and the diffusion is in the Knudsen regime, Φ is proportional to $\exp(E_a/RT)/T^{1/2}$ and $(L/R^0)^2$. In these cases the Thiele modulus increases with increasing temperature and is proportional to the ratio of substrate thickness to pore size, but is independent of the total pressure. Obviously, a higher reactant concentration in the bulk phase results in a larger value of the Thiele modulus. The total pressure can affect the Thiele modulus only when diffusion in substrate pores is in the transition or molecular diffusion regime. Normally a higher total pressure gives a larger value of the Thiele modulus because of a smaller intrapore diffusivity. Therefore, Fig. 5 shows the effects of these four experimental parameters on the deposition results of the CVI and MCVD processes.

It is obvious that in a CVI process no further densification can proceed after the pore entrance is closed by the deposit. Therefore, the densification quality depends largely on the uniformity of the deposit distribution. To obtain a more uniform densification across a preform by the isothermal CVI, the present simulation results suggest that the experimental conditions with a value of the Thiele modulus as small as possible are desired. However, a small value of the Thiele modulus corresponds to a low densification rate. In order to improve both uniformity and densification rate, development of non-isothermal CVI is therefore very important. For membrane preparation or modification by the MCVD, the experimental conditions with Thiele modulus as large as possible is preferred so that the solid product can be deposited in a very narrow zone across substrate at a rather high pore narrowing rate. The broadness of the deposition zone decreases with increasing Φ when Φ is very large. It should be pointed out that the location of the deposition zone (or the maximum deposition location) is not determined by the Thiele modulus but by the reaction orders as discussed before and some other parameters to be discussed next.

The effects of the relative intrapore diffusivity and bulk phase concentration for reactant B with respect to those for reactant A on the deposition profiles are presented in Figs 6 and 7 for both (a) the CVI and (b) MCVD processes. As shown in Figs 6(a) and 7(a), a flatter deposition profile can be achieved by increasing D_B^0 or decreasing C_B^0. Since the Thiele modulus defined here is based on reactant A, a larger value of D_B^0 means a larger overall diffusion rate for the CVI process. On the other hand, a lower value of C_B^0 indicates a smaller overall reaction rate. As previously discussed, the flatter deposition profiles with larger D_B^0 or smaller C_B^0 are due to higher diffusion rate and lower reaction rate. For the CVI, the pore closure time Θ remains the same with different values of D_B^0 [Fig. 6(a)] but decreases with increasing C_B^0 [Fig. 7(a)]. Theoretically, the following equation can be found for the (dimensionless) pore-closure time for the CVI [by integrating eq. (29) at $Z = L$]:

$$\Theta = (\gamma\Phi)^{-1}. \tag{43}$$

For the simulated CVD reaction of first order with respect to both the reactant, $\Phi = (KL^2/R^0)(C_B^0/D_A^0)$. Therefore, the variation of D_B^0 should not affect the pore-closure time which, however, should be inversely proportional to C_B^0. The simulated values of the pore-closure time are consistent with eq. (43).

For the MCVD the effects of D_B^0 and C_B^0 on the deposition results are quite different from those for

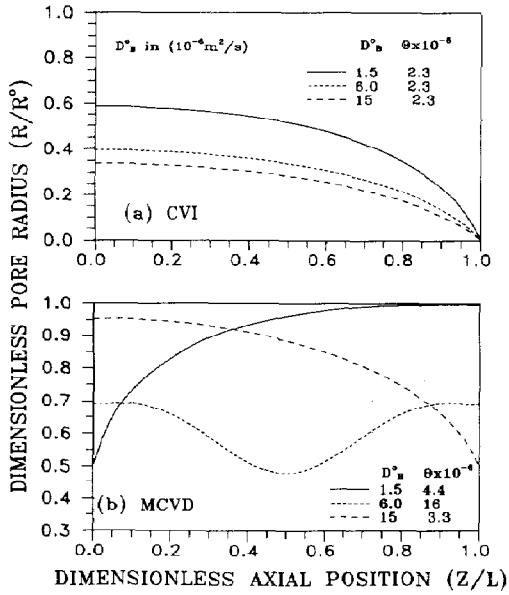

Fig. 6. Effects of relative intrapore diffusivity on the deposition profiles for (a) the CVI and (b) the MCVD (with $D_A^0 = 2.9 \times 10^{-6}$ m²/s, $C_B^0 = C_A^0 = 2.0 \times 10^{-3}$ mol/m³ and all other parameter values given in Table 3 part A).

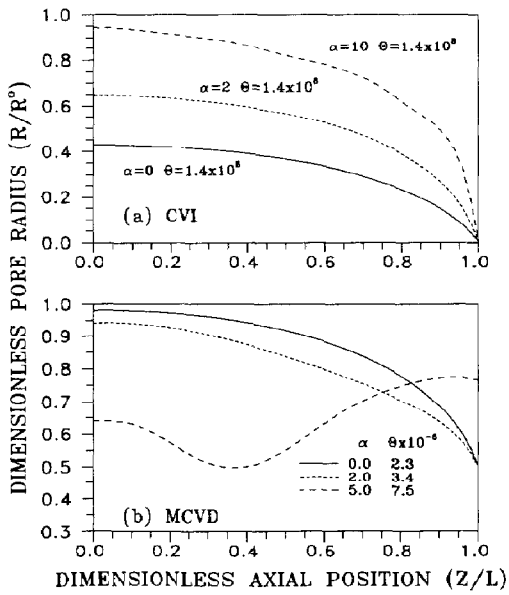

Fig. 8. Effects of total pressure drop on the deposition profiles for (a) the CVI and (b) the MCVD (with $N = 1$, $M = 1$, $\lambda_v = 1$ and all other dimensionless parameter values given in Table 3 part B).

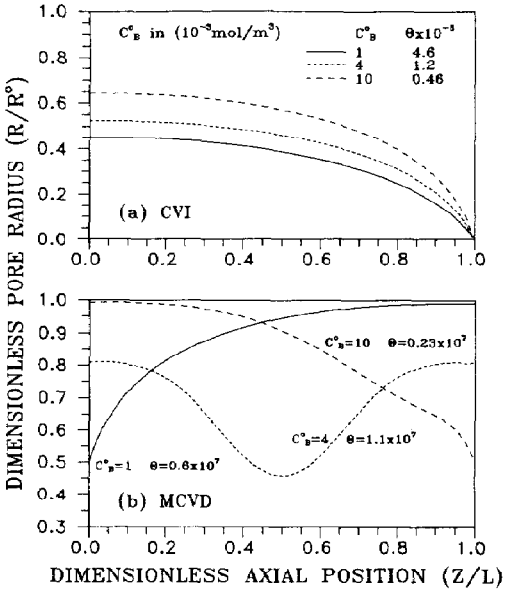

Fig. 7. Effects of relative bulk phase concentration on the deposition profiles for (a) the CVI and (b) the MCVD (with $C_A^0 = 2.0 \times 10^{-3}$, $D_B^0 = D_A^0 = 2.9 \times 10^{-6}$ m²/s and all other parameter values given in Table 3 part A).

the CVI. Firstly, with increasing D_B^0 or C_B^0 the maximum deposition location moves from the side of substrate exposed to reactant B to the other side exposed to reactant A. It is possible that the maximum deposition location is inside the substrate when λ_B ($= D_B^0/D_A^0$) or β ($= C_B^0/C_A^0$) is more close to the ratio of the stoichiometrical coefficients for reactants A and B: n_B/n_A (e.g λ_B or $\beta \approx 2$ for the simulated CVD system). It should be noted that the results presented in Figs 6 and 7 are for the case of first reaction order with respect to both the reactants. Secondly, there is no analytical relation such as eq. (43) which can be used to correlate the half pore-narrowed time to the experimental parameters for the MCVD. The simulation results presented in Figs 6(b) and 7(b) also suggest that the half pore-narrowed time is longer for the case with maximum deposition location inside substrate than that for the case with the maximum deposition located at the side of substrate.

The viscous flow in the forced-flow CVI and non-isobaric MCVD is due to the total pressure drop over the substrate. Figure 8 shows the effects of the pressure drop coefficient α, as defined in Table 1, on the deposition profiles. For the CVI process, the pore-closure time is the same for different pressure drops, as shown by the simulation results presented in Fig. 8(a). This is in agreement with the theoretical prediction by eq. (43). These results indicate that imposing a total pressure drop should not raise the CVI densification rate unless the reactant concentration in the feeding stream is increased as a result of imposing total pressure drop. The simulation results presented in Fig. 8(a), however, show that imposing a total pressure drop has unfavourable effects on the uniformity of the deposit distribution for the CVI process. A larger total pressure drop results in a less uniform deposition profile.

In a previous theoretical study (Lin, 1990b) it has been found that assuming a constant viscous flow velocity (Lin, 1990b) or constant gas permeability

(Starr, 1987) across the substrate the total pressure drop has a favourable effect on the distribution of solid deposit for the CVI process. However, for gas transport in porous media, the viscous flow velocity is generally dependent on the total pressure and, consequently, the location in the porous substrate. For example, with a constant pore radius across the substrate, solution of eqs (8) and (18) gives:

$$U = \alpha\lambda_v(D_A^0/L)(\alpha\xi + 1)^{-1/2}. \quad (44)$$

To examine these seemingly unusual unfavourable effects of the total pressure drop on the deposit distribution, let's compare the following three cases using eq. (9) (with $R = R^0$, $N = 1$ and $M = 0$): (A) eq. (9) with the third term and U in the second term omitted (the case without total pressure drop, i.e. $U = 0$); (B) eq. (9) with only the third term omitted (the case with a total pressure drop and constant U across substrate, i.e. $U \neq 0$ but $dU/dZ = 0$); (C) eq. (9) with a total pressure drop and variable U, which has the following form:

$$D_i\frac{d^2C_i}{dZ^2} - U\frac{dC_i}{dZ} = \left(K + \frac{dU}{dZ}\right)C_i. \quad (45)$$

Since $dU/dZ[= -U\alpha/2L(\alpha\xi + 1)]$ is always positive, the addition of the term dU/dZ on the right-hand side of eq. (45) is equivalent to an increase in the reaction rate, very likely resulting in an effect of steepening the deposition profile which surpasses the effect of flattening the deposition profile by the term $(-UdC_i/dZ)$ on the left-hand side of eq. (45). In fact, the simulation results show that the flatness of the reactant concentration profiles decrease in the following order: case (B), case (A) and case (C).

For the MCVD process, the simulation results presented in Fig. 8(b) shows a significant effect of the total pressure drop on the shape of the deposition profile. Figure 8(b) also shows that imposing a total pressure drop can move the maximum deposition location towards the substrate side of the lower total pressure. Again the pore narrowing rate for the deposition profile with its maximum deposition location more closed to the middle of substrate is slower than the other two deposition profiles with its maximum deposition located at substrate side. It should be noted that the results presented in Fig. 8 are calculated with a relatively large value of the ratio of viscous flow velocity to diffusivity λ_v (see Table 1). In fact, a large value of λ_v is a prerequisite to the effects of the total pressure drop on the deposition profiles. Figure 9 shows the simulated deposition profiles for the forced-flow CVI and the non-isobaric MCVD with different value of λ_v (at a constant value of $\alpha = 10$). When λ_v is smaller than 0.01 (for MCVD) or 0.001 (for CVI) the pressure drop does not influence the deposition profiles. As seen in Table 1, λ_v can be reduced by lowering P_0 (or the average total pressure) and the substrate pore radius R^0. Therefore, under experimental conditions of low average pressure and small substrate pore size such as the case given in

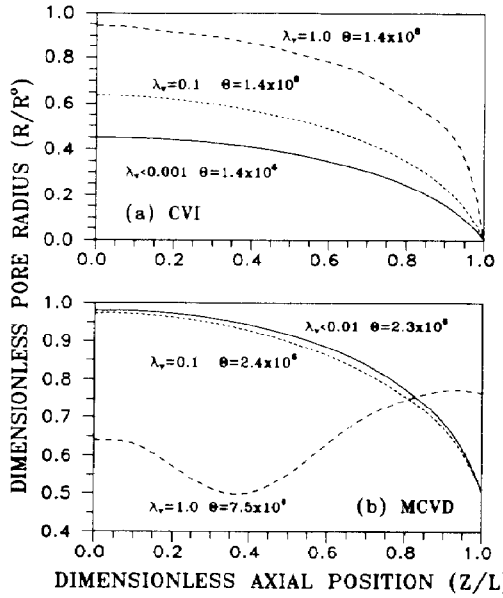

Fig. 9. Effects of the ratio of viscous flow to diffusive flow on the deposition profiles for (a) the CVI and (b) the MCVD (with $N = 1$, $M = 1$, $\alpha = 10$ and all other dimensionless parameter values given in Table 3 part B).

Table 3 ($\lambda_v \ll 0.01$) imposing a small pressure drop does not change the deposition profile.

For the isothermal CVI and the isobaric MCVD, the similar parameters that determine whether or not the total pressure (not the total pressure drop) affect the deposition results are the ratio of the Knudsen diffusivity to the molecular diffusivity ω_i (i = A and B). When ω_i is smaller than 10^{-3} it is found that variation of the total pressure does not change the deposition profiles. As ω_i is proportional to (R^0P) [see eq. (4a) and (4b)], the value of ω_i can be very small under the experimental conditions of lower total pressure and small substrate pore size such as the case listed in Table 3 (for reactant B, water vapor, $\omega_B \approx 1.6 \times 10^{-4}$). For the last parameter given in Table 1, the ratio of the reactant concentration to solid deposit concentration γ, the simulation results show the same deposition profiles for both the CVI and MCVD with different values of γ. The parameter γ only affects the pore narrowing rate which is proportional to γ, as indicated by eq. (38).

To compare the simulation results for the MCVD with the BC of zero concentration (i.e. $C_A = 0$ at $Z = 0$ and $C_B = 0$ at $Z = L$) (Carolan and Michaels, 1987; Lin *et al.*, 1989b) and the present BC of zero concentration derivative [eqs (12) and (13)], the simulated deposition profiles with the two types of BC for three cases of different reaction orders are presented in Fig. 10. For the two cases of a zero reaction order with respect to one reactant quite similar simulated deposition profiles are obtained with these two types of BC. For the case of first reaction order on both reactants the simulated deposition profile with the BC of zero concentration [Fig. 10(a)] is very different

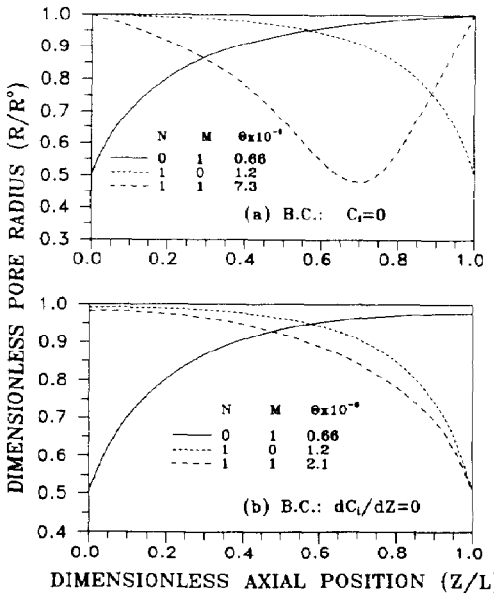

Fig. 10. Comparison of simulated deposition profiles with (a) zero concentration boundary conditions and (b) the boundary conditions of zero concentration derivatives for the MCVD process (with all the dimensionless parameter values given in Table 3 part B).

from the one with the BC of zero concentration derivative [Fig. 10(b)]. The maximum deposition location is always inside the substrate for the first type of BC, but varies from edge to inside of the substrate depending on values of other parameters for the second type of BC. It appears that the second type of BC is more suitable for such a problem of transport and reaction in porous media because the theoretical analysis using this type of BC is consistent with the experimental results which will be given in a separate paper.

CONCLUSIONS

A phenomenological mathematical model is developed to describe the one-dimensional isothermal forced-flow CVI process for material densification and the non-isobaric MCVD process for ceramic membrane preparation. The model takes into account chemical reaction and deposition, diffusion, viscous flow and change of pore geometry and transport properties, and can be readily solved by the orthogonal collocation method. It neglects details of the phase structure of deposit and assumes cylindrical pores of substrate. This model with the simulation results allows the analysis of the effects of reaction mechanism, temperature, total pressure, total pressure drop, substrate pore dimension, bulk phase reactant concentration and intrapore diffusivity on deposition results of the CVD processes in porous media.

The simulation results show that the uniformity of densification across a preform in an isothermal CVI process can be improved by: (1) using a reaction with a low reaction order with respect to the reactants; (2) decreasing the Thiele modulus by varying preform temperature, total pressure, preform pore dimension; (3) reducing the reactant concentration; (4) increasing intrapore diffusivity and (5) reducing the total pressure drop across the substrate. The maximum local densification rate is determined by the reaction rate at entrance port of a preform. Simulation results also show that in the isothermal CVI process improving the uniformity of densification is accompanied with prolonging the pore-closure time (or lowering the densification rate).

For membrane preparation and modification the simulation results suggest that the maximum deposition location, broadness of deposition zone and the pore narrowing rate can be controlled by several parameters: reaction orders, the Thiele modulus, reactant concentration in the bulk phase, diffusivity and the total pressure drop. A narrow deposition zone and a high pore narrowing rate can be achieved with the experimental conditions of large value of Thiele modulus. The maximum deposition location can be moved towards one side of the substrate disc by increasing the bulk phase concentration, intrapore diffusivity of the reactant and the total pressure (higher than a certain value) on the other side of the substrate. The maximum deposition location is more close to the substrate side exposed to the reactant with a lower reaction order.

Acknowledgements—The financial support from Dutch Ministry of Economical Affairs under the grant IOP-TK 87 A045 is very much appreciated.

NOTATION

A_i coefficient in eq. (21) for reactant i, %
A_v coefficient in eq. (26b) for total pressure, %
a_k coefficient for Knudsen diffusivity, eq. (4b), m/s
a_m coefficient for molecular diffusivity, eq. (4c), m^2 Pa/s
B_i coefficient in eq. (21) for reactant i, %
B_0 characteristic constant for porous media, m^2
B_v coefficient in eq. (26b) for total pressure, %
C_i concentration of reactant i in the substrate pore (i = A for reactant A; i = B for reactant B), mol/m^3
C_i^0 concentration of reactant i in the bulk vapour phase, mol/m^3
D_i effective intrapore diffusivity for reactant i, m^2/s
D_i^0 effective intrapore diffusivity for reactant i in the substrate pore before deposition (at $R = R^0$), m^2/s
$D_{i(m)}$ molecular diffusivity for reactant i, m^2/s
$D_{i(k)}$ Knudsen diffusivity for reactant i, m^2/s
E_i coefficient in eq. (21) for reactant i, %
H dimensionless viscous flow velocity, see Table 1
J_i flux of reactant i in pore axial direction, mol/m^2 s
K reaction rate constant, $m^{3N+3M-2}/s\,mol^{N+M-1}$

L thickness of substrate disc, m
M reaction order with respect to reactant B
M_s molecular weight of solid deposit, kg/mol
N reaction order with respect to reactant A;
N_{Bi} Biot number, %
Nc total number of internal collocation points
n_i stoichiometric coefficients for reactant i
n_s stoichiometric coefficient for solid product
P local total pressure in the substrate pore, Pa
P_0 total pressure in the low pressure side, Pa
P_1 total pressure in the high pressure side, Pa
R local radius of substrate pore, m
R^0 average radius of substrate pore before deposition, m
R_g gas constant, J/mol K
$\mathbf{R}_i$ reaction (consumption) rate of reactant i, mol/m^3 s
$\mathbf{R}_s$ formation rate of solid deposit, mol/m^2 s
t deposition time, s
U viscous flow velocity in substrate, m/s
x_i molar fraction of component i
X_i dimensionless concentration for reactant i, see Table 1
Y dimensionless total pressure, see Table 1
Z axial position of substrate pore, m

Greek letters

α pressure drop coefficient, see Table 1
β ratio of concentration of reactant B to that of reactant A, see Table 1
γ ratio of vapour concentration to solid deposit concentration, see Table 1
ε local porosity of substrate
ε^0 average porosity of substrate before deposition
θ dimensionless time, see Table 1
Θ dimensionless pore-closure time (CVI) or half-pore-narrowed time (MCVD)
λ_B ratio of effective diffusivity of reactant B to that of reactant A, see Table 1
λ_v ratio of viscous flow velocity to diffusivity ratio, see Table 1
μ viscosity of carrier gas, kg/m s
ξ dimensionless pore axial position, see Table 1
ρ density of the solid deposit, kg/m^3
τ tortuosity factor of substrate
ϕ dimensionless pore radial position, see Table 1
Φ Thiele modulus, see Table 1
ω_i ratio of Knudsen diffusivity to molecular diffusivity for reactant i, see Table 1

REFERENCES

Besmaan, T. M., Lowden, R. A., Stinton, D. P. and Staar, T. L., 1989, A method for rapid chemical vapor infiltration of ceramic composites. *J. Phys. Colloque* **50**, 229–240.

Bird, R. B., Stewart, W. E. and Lightfoot, E. N., 1960, *Transport Phenomena*, p. 559, Wiley, New York.

Brekel, C. H. J., van der, Fonville, R. M. M., Straten, P. J. M., van der and Verspui, G., 1981, CVD of Ni, TiN and TiN on complex shapes, in *Proceedings of the 8th International Conference CVD* (Edited by J. M. Blocher *et al.*), pp. 144–156. The Electrochemical Society, Pennington, NJ.

Burggraaf, A. J., Keizer, K and van Hassel, B. A., 1989, Ceramic nanostructure, materials, membranes and composite layers. *Solid State Ionics* **32/33**, 771–782.

Burggraaf, A. J. and Keizer, K., 1990, Synthesis of inorganic membranes, in *Inorganic Membranes: Synthesis, Characteristics and Applications* (Edited by R. R. Bhave), Chap. 2. van Nostrand Reinhold, New York.

Butt, J. B., 1980, *Reaction Kinetics and Reactor Design*, Chap. 1. Prentice-Hall, Englewood Cliffs, NJ.

Carnahan, B., Luther, H. A. and Wilkes, J. O., 1977, *Applied Numerical Methods*, pp. 334–347. Wiley, New York.

Carolan, M. and Michaels, J. N., 1987, Chemical vapour deposition of yttria stabilized zirconia on porous substrates. *Solid State Ionics* **25**, 207–216.

Carolan, M. and Michaels, J. N., 1990, Growth rates and mechanism of electrochemical vapor deposited yttria-stabilized zirconia films. *Solid State Ionics* **37**, 189–195.

Chiang, Y. M., Haggerty, J. S., Messner, R. P. and Demetry, C., 1989, Reaction-based processing methods for ceramic-matrix composites. *Ceramic Bulletin* **68**, 420–428.

Christin, F., Naslain, R. and Bernard, C., 1979, Thermodynamic and experimental approach of silicon carbide CVD application to the CVD infiltration of porous carbon-carbon composites, in *Proceedings of the 7th International Conference CVD* (Edited by T. O. Sedgwick and H. Lydtin), pp. 499–514. The Electrochemical Society, Pennington, NJ.

Gavalas, G. R., Megiris, C. E. and Nam, S. W., 1989, Deposition of H_2-permselective Si_2O films. *Chem. Engng Sci.* **44**, 1829–1835.

Gupte, S. M. and Tsamopoulos, J. A., 1989, Densification of porous materials by chemical vapour infiltration. *J. electrochem. Soc.* **136**, 555–561.

Hsieh, H. P., 1988, Inorganic membranes. *A.I.Ch.E. Symp. Ser.* **84**, 1–18.

IMSL User's Manual, 1987, IMSL, 2500 City West Boulevard, Houston, TX 77042.

Isenburg, A. O., 1977, Growth of refractory oxide layers by electrochemical vapor deposition (EVD) at elevated temperatures. *ECS Symp. Electrode Materials, Processes for Energy Conversion and Storage*, **77**, 572–583.

Keizer, K., Uhlhorn, R. J. R., van Vuren, R. J. and Burggraaf, A. J., 1988, Gas separation mechanisms in microporous modified γ-Al_2O_3 membranes. *J. Membrane Sci.* **39**, 258–300.

Lin, Y. S., de Haart, L. G. J., de Vries, K. J. and Burggraaf, A. J., 1989a, Modification of ceramic membranes by CVD and EVD for gas separation, catalysis and SOFC application, in *Euro-Ceramics Vol. 3—Engineering Ceramics* (Edited by G. de With *et al.*), pp. 3590–3595. Elsevier, London.

Lin, Y. S., de Vries, K. J. and Burggraaf, A. J., 1989b, CVD modification of ceramic membranes: simulation and preliminary results. *J. Phys. Colloque* **50**, 861–872.

Lin, Y. S., Fransen, P., de Vries, K. J. and Burggraaf, A. J., 1990a, Experimental study on CVD modification of ceramic membranes, in *Proceedings of the 11th International Conference CVD* (Edited by K. E. Spear), pp. 539–544. The Electrochemical Society, Pennington, NJ.

Lin, Y. S., 1990b, Analysis of CVI process for material densification using a continuous model, in *Proceedings of the 11th International Conference CVD* (Edited by K. E. Spear), pp. 532–538. The Electrochemical Society, Pennington, NJ.

Lin, Y. S., de Haart, L. G. J., de Vries, K. J. and Burggraaf, A. J., 1990c, A kinetic study on the electrochemical vapor deposition of solid oxide films on porous substrates. *J. electrochem. Soc.* **137**, 3960.

Mason, E. A., Malinauskas, A. P. and Evans, R. B. III, 1966, Flow and diffusion of gases in porous media. *J. chem. Phys.* **46**, 3199.

Mason, E. A. and Malinauskas, A. P., 1983, *Gas Transport in Porous Media: the Dustry Gas Model*, Chap. 2. Elsevier, Amsterdam.

Naslain, R., Langlais, F. and Fedou, R., 1989, The CVI-processing of ceramic matrix composites. *J. Phys. Colloque* **50**, 191–207.

Reid, R. C., Prausnitz, J. M. and Sherwood, T. K., 1977, *The Properties of Gases and Liquids*, 3rd Edition, pp. 548–549. McGraw-Hill, New York.

Rossignol, J. Y. and Naslain, J. J., 1980, Carbon–carbon titanium carbide composite materials obtained by CVI of porous carbon–carbon substrates, in *Proceedings of the 3rd European Conference CVD* (Edited by H. E. Hintermaan), pp. 162–168. Neuchatel, Switzerland.

Rossignol, J. Y., Langlais, F. and Naslain, R., 1984, A tentative modelization of titanium carbide CVI within the pore network of two-dimensional carbon–carbon composite preforms, in *Proceedings of the 9th International Conference CVD* (Edited by Mc. D. Robinson), pp. 596–614. The Electrochemical Society, Pennington, NJ.

Ruthven, D. M., 1984, *Principles of Adsorption and Adsorption Processes*, p. 137. Wiley, New York.

Smith, J. M., 1981, *Chemical Engineering Kinetics*, pp. 451–453. Wiley, New York.

Starr, T. L., 1987, Model for rapid CVI of ceramic composites, in *Proceedings of the 10th International Conference CVD* (Edited by G. W. Collen), pp. 1147–1155. The Electrochemical Society, Pennington, NJ.

Starr, T. L., 1988, Deposition kinetics in forced flow/thermal gradient CVI. *Ceram. Engng Sci.* **9**, 803–812.

Tai., N-H. and Chou, T. W., 1988, Theoretical analysis of chemical vapour infiltration in ceramic/ceramic composites. *Mat. Res. Soc. Symp. Proc.* **120**, 185–192.

Tai., N-H. and Chou, T. W., 1989, Analytical modelling of chemical vapour infiltration of ceramic composites. *J. Am Ceram. Soc.* **72**, 414–420.

Villadsen, J. and Michelsen, M., 1978, *Solution of Differential Equation Models by Polynomial Approximation*, Chaps 2–4. Prentice-Hall, Englewood Cliffs, NJ.

APPENDIX

Derivation of collocation equations

The variables of X_i and Y along pore axial position are approximated by the following polynomial with N being the total number of the internal collocation points:

$$P(\xi) = \sum_{j=1}^{N+2} L_j(\xi) P_j \tag{A1}$$

where P represents anyone of X_i and Y with

$$L_j(\xi) = \prod_{\substack{i=1 \\ (i \neq j)}}^{N+2} [(\xi - \xi_i)/(\xi_j - \xi_i)] \tag{A2}$$

and ξ_j is the jth zero of the orthogonal polynomial defined by Villadsen and Michelsen (1978).

From eq. (A1) the first- and second-order derivatives can be discretized as:

$$\left.\frac{dP}{d\xi}\right|_k = \sum_{j=1}^{N+2} \mathbf{B}_{kj} P_j \quad k = 1, 2, \ldots, N+2 \tag{A3}$$

$$\left.\frac{d^2P}{d\xi^2}\right|_k = \sum_{j=1}^{N+2} \mathbf{A}_{kj} P_j \quad k = 1, 2, \ldots, N+2 \tag{A4}$$

where k represents k the collocation point along the pore axial direction. The discretization matrices $\mathbf{A}_{kj}$ and $\mathbf{B}_{kj}$ as well as the values of ξ_j were computed using the algorithm suggested by Villadsen and Michelsen (1978).

Discretizing eq. (29) gives:

$$\frac{d\phi_k}{d\theta} = -f_s(X_{A,k}, X_{B,k}) \quad k = 1, 3, \ldots, N+2 \tag{A5}$$

with: $\phi_k = 1$ at $\theta = 0$. (A6)

Discretization of eq. (26) yields:

$$\sum_{j=1}^{N+2} [(A_v)_k \mathbf{A}_{kj} + (B_v)_k \mathbf{B}_{kj}] Y_j = 0 \quad k = 2, 3, \ldots, N+1 \tag{A7}$$

with

$$Y_1 = 0 \tag{A8}$$

$$Y_{N+2} = 1. \tag{A9}$$

The coefficients of $(A_v)_k$ and $(B_v)_k$ in eq. (A7) can be written as:

$$(A_v)_k = \phi_k \tag{A10}$$

$$(B_v)_k = 2 \sum_{j=1}^{N+2} \mathbf{B}_{kj} \phi_j. \tag{A11}$$

Equation (21) can be discretized to

for reactant A:

$$\sum_{j=1}^{N+2} [(A_A)_k \mathbf{A}_{kj} + (B_A)_k \mathbf{B}_{kj} + \delta_{kj}(E_A)_k](X_A)_k - f_A(X_{A,k}, X_{B,k}) = 0$$
$$k = 2, 3, \ldots, N+1 \tag{A12}$$

with:

$$\left.\begin{aligned} &(X_A)_{N+2} = 1 \\ &\sum_{j=1}^{N+2} \mathbf{B}_{1,j}(X_A)_j = 0 \end{aligned}\right\}$$
for both the CVI and MCVD processes (A13)

and for reactant B:

$$\sum_{j=1}^{N+1} [(A_B)_k \mathbf{A}_{kj} + (B_B)_k \mathbf{B}_{kj} + \delta_{kj}(E_B)_k](X_B)_k - f_B(X_{A,k}, X_{B,k}) = 0 \quad k = 2, 3, \ldots, N+1 \tag{A14}$$

with:

$$\left.\begin{aligned} &(X_B)_{N+2} = 1 \\ &\sum_{j=1}^{N+2} \mathbf{B}_{1,j}(X_B)_j = 0 \end{aligned}\right\}$$ for the CVI process (A15)

$$\left.\begin{aligned} &\sum_{j=1}^{N+2} \mathbf{B}_{N+2,j}(X_B)_j = 0 \\ &(X_B)_1 = 1 \end{aligned}\right\}$$ for the MCVD process (A16)

with

$$\delta_{kj} = \begin{cases} 0 & k \neq j \\ 1 & k = j. \end{cases} \tag{A17}$$

The coefficients $(A_i)_k$, $(B_i)_k$ and $(E_i)_k$ (i = A or B) in eqs (A13) and (A15) are related to ϕ_k and Y_k by:

$$(h_i)_k = (\omega_i + 1)/[\omega_i \phi_k (\alpha Y_k + 1)^{1/2} + 1] \tag{A18}$$

$$(A_i)_k = \lambda_i (\phi_k)^2 (h_i)_k \tag{A19}$$

$$(a_i)_k = \lambda_i (h_i)_k \phi_k [(h_i)_k/(\omega_i + 1) + 2] \tag{A20}$$

$$(b_i)_k = 0.5\phi_k [\omega_i/(\omega_i + 1)](\lambda_i/\lambda_v)(h_i)_k^2 - \phi_k \tag{A21}$$

$$H_k = -\phi_k^2 \frac{\alpha \lambda_v}{(\alpha Y_k + 1)^{1/2}} \sum_{j=1}^{N+2} \mathbf{B}_{kj} Y_j \tag{A22}$$

$$(B_i)_k = (a_i)_k \sum_{j=1}^{N+2} [\mathbf{B}_{kj} \phi_j + (b_i)_k H_k] \tag{A23}$$

and

$$(E_i)_k = -2H_k \sum_{j=1}^{N+2} \mathbf{B}_{kj} \phi_j - \phi_k \sum_{j=1}^{N+2} \mathbf{B}_{kj} H_j. \tag{A24}$$

Computation algorithm

(1) Calculate the zeros of the orthogonal polynomial and the discretization matrices $\mathbf{A}_{kj}$ and $\mathbf{B}_{kj}$ (with $N = 8$, $\alpha = 0.5$ and $\beta = 0.5$) using the algorithm given by Villadsen and Michelsen (1978) and input all the simulation parameters and initial values: $\phi_k = 1$ ($k = 1, 2, \ldots, 10$); (2) find $(X_A)_k$, $(X_B)_k$ and Y_k ($k = 1, 2, \ldots, 10$) by solving 30 algebraic eqs (A7)–(A9) and (A13)–(A16) using IMSL routine NEQNF; (3) evaluate the integration step of $\Delta\theta$ so that each integration step corresponds to an increment in ϕ of about 1/2000; (4) calculate new deposition profile of ϕ_k ($k = 1, 2, \ldots, 10$) by integrating eq. (A5); (5) repeat steps (2), (3), (4) until the minimum ϕ_k is about 0.5 ± 0.005 (for the MCVD) or 0 ± 0.005 (for the CVI).